Journal of Hazardous Materials 182 (2010) 64–74

Contents lists available at ScienceDirect

Journal of Hazardous Materials

journal homepage: www.elsevier.com/locate/jhazmat

Aqueous removal of diclofenac by plated elemental iron: Bimetallic systems

Antoine Ghauch*, Hala Abou Assi, Sara Bdeir

American University of Beirut, Faculty of Arts and Sciences, Department of Chemistry, P.O. Box 11-0236, Riad El Solh, 1107-2020 Beirut, Lebanon

ARTICLE INFO

Article history:
Received 12 April 2010
Received in revised form 21 May 2010
Accepted 28 May 2010
Available online 8 June 2010

Keywords:
Diclofenac
Emerging contaminants
Fe^0/H_2O systems
Bimetallics
HPLC/MS

ABSTRACT

The aqueous removal of diclofenac (DF) by micrometric iron particles (Fe^0) and amended Fe^0 ($Me^0(Fe^0)$) under oxic and anoxic conditions was investigated. Bimetallic systems were obtained by plating the surface of Fe with Co, Cu, Ir, Ni, Pd and Sn. Experimental results confirmed the superiority of ($Me^0(Fe^0)$) for DF removal except for IrFe (oxic) and SnFe (anoxic). Under anoxic conditions, Pd was by far the most efficient plating element followed by Ir, Ni, Cu, Co and Sn. However, under oxic conditions, Pd and Cu showed almost the same efficiency in removing DF followed by Ni, Co, Sn and Ir. Oxidative and reductive DF transformation products were identified under oxic and anoxic conditions respectively. In some systems (e.g. CoFe and SnFe oxic/anoxic; PdFe oxic; NiFe anoxic), no transformation products could be detected. This was ascribed to the nature of the plating element and its impact on the process of the formation of metal corrosion products (MCPs). MCPs are known for their high potential to strongly adsorb, bond, sequestrate and enmesh both the original contaminant and its reaction products. Obtained results corroborate the universal validity of the view, that aqueous contaminants are basically removed by adsorption and co-precipitation.

1. Introduction

During the last decade several studies have evidenced the broad spreading of emerging contaminants (mostly pharmaceuticals and personal care products) in the environment, especially in municipal [1], surface [2], ground [3] and even drinking water [4,5]. Diclofenac (DF) (2-(2,6-dichloranilino)phenylacetic) is one of the most consumed analgesic drug. Being slightly biodegradable, it is often detected in rivers, influents and effluents of waste water treatment plants (WWTP) in several countries (e.g. Brazil, Germany, Sweden and USA) [5–8]. Recently, DF has been shown to interfere with the biochemical functions of fish and lead to tissue damage even at environmentally relevant concentrations [9]. Therefore, DF highly charged effluents (e.g. hospitals and drug manufacturing industry effluents) should be treated prior to their release into rivers and surface waters.

Many conventional remediation methods are too costly for extensive deployment in small municipalities and in the developing world. Therefore, affordable technologies using low cost materials and matching or exceeding the capability of conventional remediation technologies are needed. Such affordable technologies will replace current hospital WWTP based on coagulation-floculation and flotation that have been proven inefficient for many pharmaceuticals [10]. Several approaches have been tested for DF removal including photo-Fenton [11], ozonation [12], and sonolysis [13]. Presently, no report on testing the suitability of metallic iron (Fe^0 and amended Fe^0) for aqueous DF removal could be found.

Microscale iron particles (Fe^0) and amended iron particles ($Me^0(Fe^0)$) have been shown very efficient for the aqueous removal of several organic [14–17] and inorganic [18–23] compounds. Four main mechanisms are reported for the removal process are: (1) contaminant adsorption on Fe^0 surface or at the surface of their corrosion products [24–29]; (2) contaminant co-precipitation with metal corrosion products (MCPs) [20,30,31,32], (3) contaminant oxidation within the oxide layer [33,34], and (4) contaminant reduction including catalytic hydrodehalogenation [35–37]. The hart fact that oxidation of some contaminants and reduction others were reported challenges the prevailing view considering Fe^0 as a reducing agent as discussed below. Redox processes may precede or follow contaminant enmeshment/sequestration (co-precipitation) in the matrix of transforming MCPs [17,38]. Ideally, reaction products are released into the bulk solution. However, because of the strong adsorptive properties of native MCPs for all contaminants (chemicals and pathogens), quantitative release of reaction products is not likely to occur. Based on this observation, the importance of the discussion on the toxicity of reaction products was questioned and Fe^0 was proposed as universal material for water treatment [39]. The logical consequence of recent works of Noubactep and his colleagues is that DF and other emerging contaminants will be removed by well-designed Fe^0 filters. One of the most important open issues is the reactivity of used materials [40].

* Corresponding author. Tel.: +961 1 350 000; fax: +961 1 365 217.
E-mail address: ag23@aub.edu.lb (A. Ghauch).

0304-3894/$ – see front matter © 2010 Elsevier B.V. All rights reserved.
doi:10.1016/j.jhazmat.2010.05.139

The present study tests the possibility of using bimetallic systems for aqueous DF removal.

Depositing a more electropositive metallic element on the surface of iron particles (plating) is known to increase Fe^0 corrosion rate through the formation of a galvanic cell [35,41–43] thereby the growth of an oxide layer responsible for contaminant enmeshment is sustained [17]. The view that atomic hydrogen adsorbed at the surface of the plating element (H_{ads}) is the primary mechanism of dehalogenation reactions has been recently revisited [17,37,44]. Ghauch and co-workers [44] demonstrated that dechlorination of clofibric acid (CLO) by PdFe was delayed while iron corrosion was accelerated by addition of MnO_2. While accelerating iron corrosion, MnO_2 retards the availability of "free" MCPs. No quantitative CLO removal was observed in the initial stage of the experiment, confirming the working hypothesis that the abundance of in situ generated MCPs was the primarily cause of CLO removal. It is clear that Fe^0 ($E^0 = -0.44$ V) oxidation by MnO_2 ($E^0 = 1.23$ V) is more favorable than oxidation by H/H_2 ($E^0 = 0.00$ V). However, the experimental evidence that quantitative CLO removal is coupled to the abundance of MCPs shows that amended Fe^0 will favor contaminant removal regardless from any redox process. Additionally, Noubactep (2009) demonstrated that the plating element is a concurrent to any reducible contaminant for Fe^0 oxidation. Altogether, the prevailing view that quantitative abiotic contaminant reduction is coupled with aqueous Fe^0 oxidative dissolution [45,46] was a "broad consensus" [47] and is inconsistent with many experimental and field observations [48,49].

This study was designed to confirm the feasibility of metallic iron to enhance microbial decontamination of wastewaters using DF as pharmaceutical compound model by performing experiments under both oxic and anoxic conditions. The specific objective was to test several plating agents and identify the most efficient to sustain iron corrosion, and thus long-term DF removal. The identification of DF reaction products under oxic/anoxic conditions helps in discussing the DF removal mechanism.

2. Experimental methods

2.1. Materials

Palladium (II) acetate ($[Pd(C_2H_3O_2)_2]$ (Pd assay 47%)) and nitrogen flushed micrometric iron particles (325 mesh) were purchased from Fluka (USA). Nickel (II) chloride ($NiCl_2$) and Tin (II) chloride anhydrous ($SnCl_2$) were from Aldrich (USA). Cobalt (II) chloride, ($CoCl_2{\cdot}6H_2O$), Iridium (IV) chloride (≥99.9% trace metals basis) ($IrCl_4{\cdot}H_2O$), Copper (II) sulfate monohydrate ($CuSO_4{\cdot}H_2O$) and diclofenac sodium ($C_{14}H_{10}Cl_2NO_2Na$) were obtained from Sigma (USA). Methanol (HPLC grade), formic acid and acetone (analytical reagent) were acquired from Riedel de Haen (Germany). Hydrochloric acid (HCl) and Whatman No. 1 filter papers ($\phi = 3$ cm, pore size 15 μm) were purchased from Prolabo (France). PTFE acrodisc syringe filters ($\phi = 13$ mm, pore size = 0.45 μm) were obtained from Jaytee Biosciences (UK). Double distilled water was used for all dilutions; deionized water for HPLC/MS analysis. Nitrogen and zero air gases used for purging solutions were obtained in cylinders however, pure N_2 used for the HPLC/MS was provided from a nitrogen-hydrogen generator (Clained HG 2200, Model HG 2200 B, Italy).

2.2. Procedures

2.2.1. Metallic particles preparation

Based on their standard reduction potentials (Table 1) [50], all catalysts were deposited on the surface of iron particles by simple metal displacement reaction in deoxygenated solutions in order to avoid the formation of metallic oxides at an early stage before any contact with the aqueous reactive medium (Eq. (1)).

$$\frac{n}{2}Fe^0 + Me_1{}^{n+} \rightarrow \frac{n}{2}Fe^{2+} + Me_1{}^0(Fe^0) \quad \text{bimetallics} \tag{1}$$

where $Me_1{}^0$ is the metal to be plated, n its valence.

Based on previous work done by Bransfield and co-workers [51] and Cwiertny and co-workers [52], PdFe, NiFe, IrFe, CoFe, SnFe and CuFe were prepared by weighing an equivalent amount of 47 μmol of each catalyst per gram of Fe^0 in order to ensure that the additive loadings were constant (Table 1). After dissolution of the corresponding salts in acetone (for Pd) or 0.01 M HCl (for Ni, Ir, Sn, Co and Cu), 1.0 g of acid washed iron powder (20 mL 1 M HCl) was added to the Pyrex vial to form a slurry-like material. After 5 min of mixing metal samples were then filtered, rinsed three times with deoxygenated double distilled water and transferred along with the filter paper to one of the Pyrex recipient of the freeze dryer (Labconco, USA) for 2–3 h to remove humidity traces. The filtrate was recuperated and stocked in the refrigerator for atomic absorption spectroscopy analysis (Thermo labsystems Solaar) to check that the corresponding metals were deposited on the surface of iron particles as previously described [53,54].

2.2.2. Batch experiments

DF solutions (32 μM) were daily prepared by simple dissolution in double distilled water of the corresponding sodium salt. The resultant solutions were filtered (Nylon membrane of 0.45 μm pore size) and stocked in amber bottles to avoid photo-degradation. The concentration of dissolved oxygen measured with a portable oxygen meter (Thermo Scientific Orion, USA) in the double distilled water used was about 8 mg L^{-1}. Reactions were realized at room temperature under both oxic and anoxic conditions. The nomenclature oxic vs. anoxic conditions is preferred to aerobic vs. anaerobic because the former is more general and refers to the redox properties in general while the later is limited to the molec-

Table 1
Theoretical standard reduction potentials for metal catalysts and their corresponding salt masses (equivalent 47 μmol) used for the synthesis of ($Me^0(Fe^0)$). Electrode potentials are arranged in decreasing order of E^0 [49].

M^{n+}/M	Electrochemical reaction	E^0 (V)	Salt	Mass × 10^{-3} (g)
Pd^{II}/Pd^0	$Pd^{2+} + 2e^- \rightleftharpoons Pd^0$	0.915	$Pd(C_2H_3O_2)_2$	10.6
Ir^{IV}/Ir^0	$Ir^{4+} + 4e^- \rightleftharpoons Ir^0$	0.835	$IrCl_4$	15.8
O_2/H_2O	$O_2 + 4H^+ + 4e^- \rightleftharpoons 2H_2O$	0.81	–	–
Fe^{III}/Fe^{II}	$Fe^{3+} + e^- \rightleftharpoons Fe^{2+}$	0.77	–	–
Cu^{II}/Cu	$Cu^{2+} + 2e^- \rightleftharpoons Cu^0$	0.341	$CuSO_4{\cdot}H_2O$	11.8
Ni^{II}/Ni^0	$Ni^{2+} + 2e^- \rightleftharpoons Ni^0$	0.339	$NiCl_2$	6.1
H^+/H_2	$2H^+ + 2e^- \rightleftharpoons H_2$	0.000	–	–
Sn^{II}/Sn^0	$Sn^{2+} + 2e^- \rightleftharpoons Sn^0$	−0.141	$SnCl_2$	9.0
Co^{II}/Co^0	$Co^{2+} + 2e^- \rightleftharpoons Co^0$	−0.282	$Co(Cl)_2{\cdot}6H_2O$	11.2
Fe^{II}/Fe^0	$Fe^{2+} + 2e^- \rightleftharpoons Fe^0$	−0.440	–	1000

Theoretical standard reduction potentials for metal catalysts and their corresponding salt masses (equivalent 47 μmol) used for the synthesis of ($Me^0(Fe^0)$). Electrode potentials are arranged in decreasing order of E^0 [50].

ular oxygen content [55,56]. A previously described apparatus was used to study DF elimination kinetics [53,54] in the aim to keep the same experimental conditions (reactor shape, shaking device, etc.) allowing comparison of results on a case-to-case basis. In order to insure saturated air solution for oxic conditions, comparative experiments were realized at open atmosphere however with air sparging solution. The results did not show any significant difference with experiments occurring under open atmosphere without air sparging. Accordingly, all oxic experiments were realized in an open atmosphere reactor without air sparging. As for anoxic conditions, all solutions were sparged with nitrogen before adding the metallic systems for 15 min in order to assume complete dissolved oxygen escape. Furthermore the nitrogen flow was maintained constant throughout the reaction in order to avoid any atmospheric oxygen diffusion into the reactive medium. The pH was measured using a pH meter equipped with a micro-combination pH electrode (Thermo Scientific, USA). Two-point calibrations (pH 4, 7) were performed before measurements and for multiple samples to insure accurate pH data. No buffer was used throughout the experiments however a slightly basic pH was noticed for all starting solutions (pH_i) due to the near neutral pH of the double distilled water used ($7.5 < pH_i < 8.5$).

Prior to each experiment and before the addition of any metallic system, a reference of 0.5 mL was withdrawn from each vial for kinetic studies. For an iron load of about $\rho_m = 40\,g\,L^{-1}$ used, the calculated ratio of diclofenac to bimetallics was about 1/22,185 mol/mol. Samples (0.5 mL) were taken at 10 min intervals for 1 h then 30 min until 2 h, filtered through a PTFE syringe filter disc (0.45 μm) directly into the 1.5 mL HPLC Agilent vials then stored in the refrigerator at 4 °C before analysis. Experiments were repeated twice for reproducibility measurements.

2.2.3. Metallic systems characterization

An XRD instrument (Bruker) was used to characterize fresh and used iron particles. The results obtained were similar to our previous investigations on micrometric iron particles [57]. Despite the low sensitivity of the XRD technique, only traces of Fe_3O_4 were detected on used iron particles proving the formation of MCPs during the reaction.

PIXE (particle induced X-rays emission) and RBS (Rutherford back-scattering) techniques were also used for the characterization of fresh and used metallic systems (Fe and CuFe). PIXE and RBS experiments were carried out by using 3 MeV proton beam delivered by a NEC 1.7 MV 5-SDH tandem accelerator (Lebanese Atomic Energy Commission). The beam (~3 mm diameter) hit the target at 0°. X-ray emission from targets was detected using a Si(Li) detector. With 12.7 μm thick Be window and 165 eV measured full width at half maximum, the energy resolution was set at 5.9 keV. For RBS measurements, a silicon PIPS detector situated at 165° referring to the beam direction was used. A detailed description of the experimental setup has been reported elsewhere [58]. The PIXE and RBS spectra were treated using GUPIX and SIMNRA codes, respectively.

2.2.4. LC–MS analysis

The quantitative analysis of DF and the identification of its transformation products were carried out on an Agilent Series 1100 liquid chromatograph coupled to a diode array detector (DAD) and an extra capacity ion trap mass selective detector (MSD-XCT). The latter is equipped with an atmospheric pressure photo-ionization (APPI) source and scanned a mass/charge ratio ranging from 100 to 2200 *m/z*. For signal enhancement, triple distilled acetone was used as dopant to increase the ionization yield [59,60] thereby lowering the limit of detection of the instrument. Acetone was directly introduced into the ionization chamber of the mass spectrometer after mixing with eluent using a Tee and a micro-infusion syringe pump (kd Scientific Massachusetts, USA) at a flow of 1 μL min^{-1}. The chromatographic separations were achieved on a Discovery C_{18} reversed phase column (5 μm; 4.6 i.d. × 250 mm long) coupled to a security guard column HS C_{18} (5 μm; 4.0 i.d. × 20 mm long, Supleco, USA) all maintained at 30 °C during analysis. Chromatographic elution conditions are fixed as follow: the eluent was a mixture of 80/20 MeOH/Formic acid 0.1% (v/v) with a flow rate of about 0.9 mL min^{-1}. The system was controlled by the HPLC/MSD ChemStation software version A.09.03.

3. Results and discussion

3.1. Reactivity of bimetallic systems

3.1.1. Anoxic conditions

Fig. 1 depicts the kinetic profiles of aqueous DF removal and evidences the superiority of PdFe over other bimetallic systems. In the PdFe system, 80% DF removal is achieved within 10 min and complete removal after 2 h. A significant fluctuation in the representative time course in the range of 20–100 min can be noticed. The large variation of the standard deviations for data corresponding to the experimental phase between 20 and 100 min can be attributed to the complexity of the removal process in the system [31,32,61]. Accordingly, the system is far from any steady state which is characterized by a better reproducibility of results. Processes yielding DF removal are those yielding to the formation and transformation of MCPs [62,63]. The same trend can also be noticed with the other bimetallics (CoFe, SnFe, CuFe, NiFe and IrFe) within almost the same time scale. For IrFe, it is obvious that a real steady state was not yet achieved at the end of the experiment.

It is interesting to notice that SnFe showed the least DF removal. Its removal efficiency was even worst than that of Fe^0 alone. For this particular bimetallic system, DF removal occurs during the first 20 min of contact and no additional removal was noticed through the end of the experiment. In contrast, DF removal was progressive

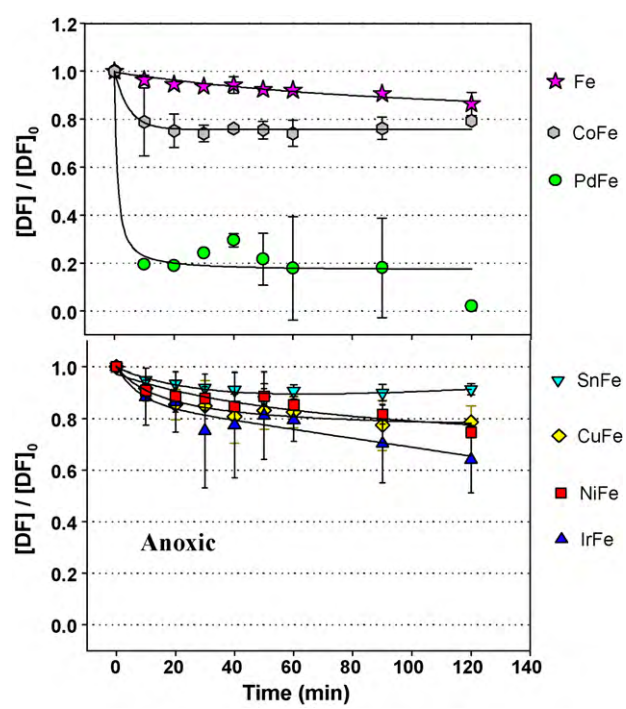

Fig. 1. Time courses illustrating the loss of DF from solution as a result of reaction with Fe^0 and ($Me^0(Fe^0)$) in anoxic solutions. Experimental conditions: $[DF]_0 = 32\,\mu M$, $pH_i = 7.5–8.5$, $\rho_m = 40\,g\,l^{-1}$, reactor volume 20 ml, room temperature. The solid lines reflect best fits to the concentration of DF based on exponential decay. Vertical bars represent standard deviations of the means.

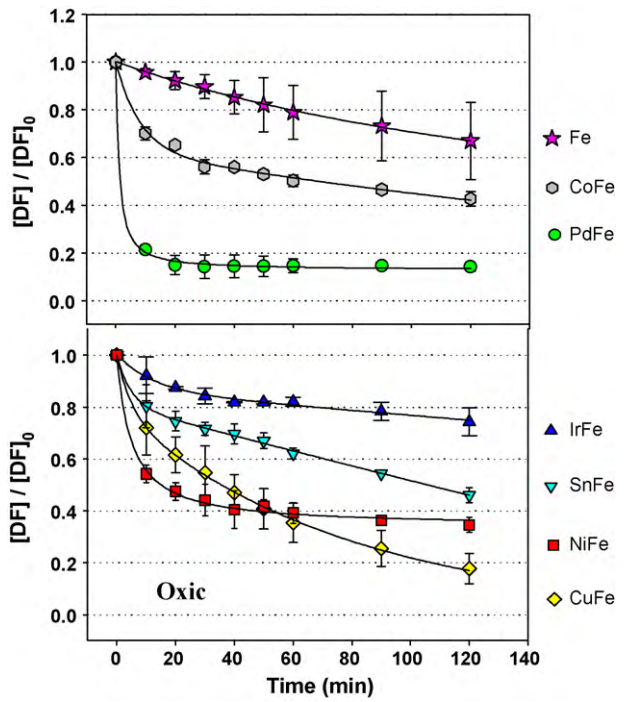

Fig. 2. Time courses illustrating the loss of DF from solution as a result of reaction with Fe^0 and ($Me^0(Fe^0)$) in oxic solutions. Experimental conditions: $[DF]_0 = 32\ \mu M$, $pH_i = 7.5–8.5$, $\rho_m = 40\ g\ l^{-1}$, reactor volume 20 ml, room temperature. The solid lines reflect best fits to the concentration of DF based on exponential decay. Vertical bars represent standard deviations of the means.

throughout the experiment in the Fe^0/H_2O system. Discussing the reason for the less reactivity of SnFe is beyond the present work, it is sufficient to consider that Sn is not a suitable plating element to sustain aqueous Fe^0 reactivity.

For IrFe, NiFe and CuFe bimetallics, one can notice that DF removal occurs to an extent of 38%, 23% and 21% respectively after 2 h of reaction. Finally, the decreasing order of bimetallics reactivity over 2 h of reaction toward DF under anoxic conditions is:

PdFe >>> IrFe > NiFe ≈ CuFe > CoFe ≈ *Fe* > SnFe.

3.1.2. Oxic conditions

Fig. 2 depicts the time dependence of DF removal by Fe^0 and ($Me^0(Fe^0)$) under oxic conditions. Again, DF removal was rapid for the first 10 to 40 min after contact with metallic systems. PdFe shows an outstanding reactivity, followed by CuFe, NiFe, CoFe, SnFe and IrFe. However, unlike under anoxic conditions, where 100% of DF removal was reached e.g. PdFe, DF was not totally removed after 2 h of reaction.

Fig. 2 also shows a better reproducibility of data (error bars) than those observed under anoxic conditions for most of the bimetallics previously investigated (Fig. 1). Furthermore, one can notice that for PdFe and NiFe bimetallics, a pseudo steady state in DF removal is achieved after 10 and 40 min respectively.

The last important feature from Fig. 2 is that the IrFe system is less reactive toward DF removal than Fe^0. Thus, the decreasing order of bimetallics reactivity over 2 h under oxic conditions was:

PdFe ≈ CuFe > NiFe > CoFe > SnFe > Fe > IrFe.

3.2. Oxic vs anoxic

In order to compare the reactivity over 2 h of all bimetallics regarding the presence or the absence of oxygen into the solutions,

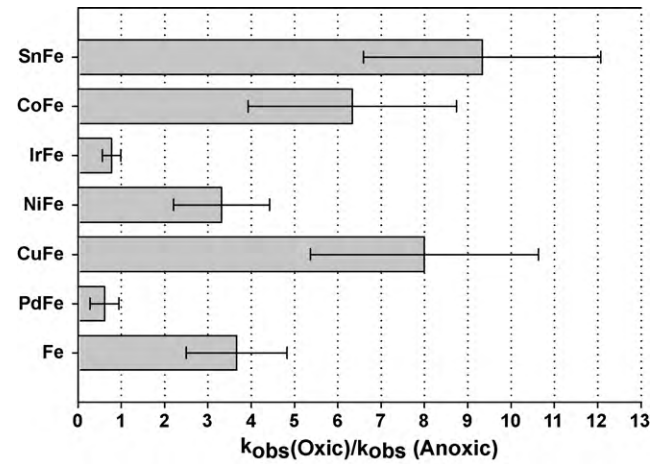

Fig. 3. Bar graph showing the ratio of k_{obs} calculated for each of the metallic catalysts used under oxic conditions to the k_{obs} values of their similar systems calculated under anoxic conditions. k_{obs} is the slope of the graph obtained by plotting $\ln(C/C_0)$ vs time of reaction.

the experimentally observed removal rates k_{obs} were calculated by plotting $\ln(C/C_0)$ vs reaction time. In that case, all curves show good agreement with pseudo-first order kinetic model (except for PdFe oxic) in which k_{obs} is the slope of the corresponding decreasing line. To get more accuracy in the k_{obs} values calculated, the whole reaction time (e.g. 2 h) was used. The rationale of this relies in (i) covering a maximum number of DF half-lives for all bimetallics tested and by (ii) taking into accounts the loss in bimetallics efficiency with time after "catalyst exhaustion". As it can be noticed from Fig. 3, dissolved oxygen (DO) has the highest impact on the reactivity of SnFe (9.3) followed by CuFe (8.0), CoFe (6.3), Fe (3.7) and NiFe (3.3). The digits in parentheses represent the values of the oxic:anoxic ratio of k_{obs} for the bimetallic systems. In contrast, DO seems to slow down the reactivity of PdFe (0.6) and IrFe (0.7) by decreasing their corresponding k_{obs} values. This might be due to their positive redox potential (Table 1) providing them an extreme initial reactivity toward DO being rapidly covered by relative dense oxide scales. Those inhibit fast DF removal compared to anoxic conditions where metallic surface oxidation is progressive and the surface coverage with oxide scales delayed.

The above presentation could help to answer the question whether the oxide scale on iron is a diffusion barrier or an impervious layer for DF which is supposedly reduced at the surface of Fe^0. The fact that almost all plating elements accelerated corrosion and favored DF removal has already confirmed the beneficial role of the oxide scale in the process of aqueous contaminant removal. It is also obvious that the initial oxide scale is a path as it is porous [62,64]. This initial path (porous layer) could be transformed to a barrier (impervious or compact layer) depending on the relative kinetics of two fundamental processes: (1) the Fe^0 further dissolution and (2) the oxide scale growth [64]. Accordingly, the observed differential behavior of plating elements is a reflect of their impact on the transformation of the initial oxide scale from a path to a barrier.

It is well-documented that the transformation of an oxide scale on Fe^0 from a path to a barrier depends primarily on the precipitation rate of the species forming the scale (here iron hydroxides). As the Fe^0 surface corrodes under the scale, corrosion continuously undermines the scale [64]. Thereby, voids or pores are created and are progressively filled up by the ongoing precipitation. If the rate of precipitation at the Fe^0 surface is superior to the rate of Fe^0 dissolution, dense protective scales form (case 1). Similarly, if Fe^0 dissolution undermines the newly formed scale faster than precipitation can fill in the voids, a porous scale forms (path) (case 2). The

presentation above suggests that PdFe and IrFe exhibit case 2 under anoxic conditions and case 1 under oxic conditions. All other plating elements exhibit case 1 under both anoxic and oxic conditions.

3.3. Rationale of MCPs formation

The argumentation regarding the kinetics of Fe^0 corrosion and oxide scales growth (as a path and/or as a barrier) corroborates the concept introduced by Noubactep [48,49,65,66] and recently validated by Ghauch and co-workers [44]. In fact, when metallic cations $Me_1{}^{n+}$ are being plated on the surface of iron particles, the first reaction is the deposition of the corresponding metal on their surface as $Me_1{}^0$. However, the formation of porous oxide scales on Me is an instantaneous phenomenon following metal immersion (see Eqs. (2)–(16)). Accordingly, $Me_1{}^{n+}$ can be entrapped into the oxide film after migration and be further reduced to $Me_1{}^0$ within the film [38]. $Me_1{}^0$, inside the oxide layers constituted of different kind of MCPs, can strongly promote DF removal via different routes.

As a result of these observations, one can confirm that DO plays an important role in the elimination of DF at neutral and near neutral pH solution without any prior solution buffering. pH profile curves presented in Fig. 4 shows a drop of the initial pH (pH_i) about almost 2.0 pH unit. This may create on the surface of the heterogeneous catalyst a micrometric zone being very acidic (pH < 4.5) which can favor the formation of hydroxyl radicals and consequently the appearance of DFo as reaction product (DFo: Hydroxylated DF, see next section). Those radicals cannot be formed in Fe^0/H_2O systems at circumneutral pH values (pH 6–8) as reported earlier [33,34]. It can also be noticed that after the first 10 min of reaction and over 2 h, a general slightly increasing trend in the pH is shown due to oxygen reduction in aqueous medium. The presence of DO indirectly favors the formation of scales of mixed oxides including FeOOH, Fe_2O_3 and Fe_3O_4 [64,67,68] after a primarily iron dissolution process (passivation, Eq. (2)) followed by depassivation (Eqs. (3)–(5)). However, under circumneutral pH conditions the production of dihydrogen decreases progressively

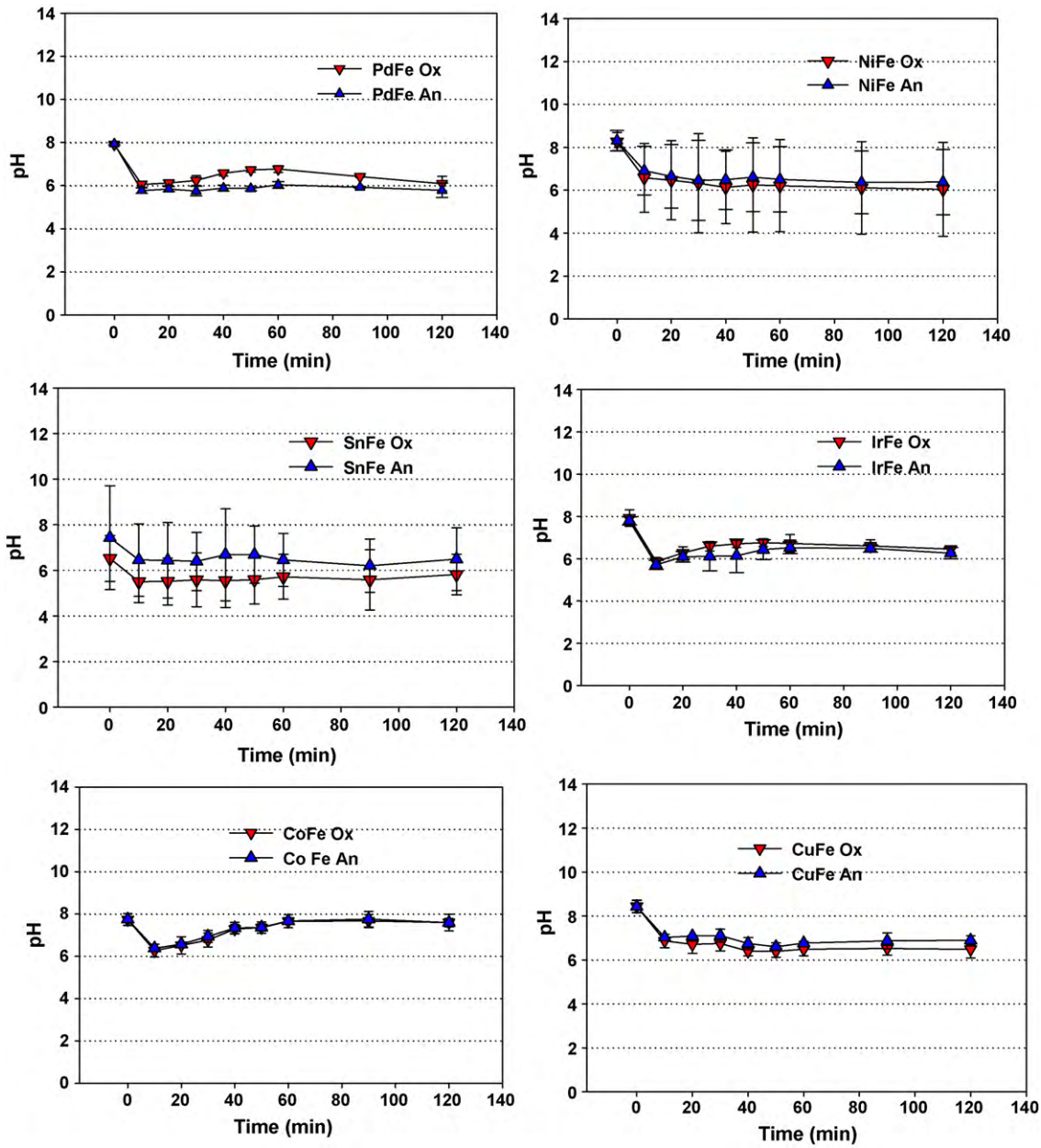

Fig. 4. pH variation during the treatment of DF solutions with different bimetallic systems. All experimental conditions are the same as in Figs. 1 and 2.

(Eq. (6)) therefore O_2 reduction is more favorable (Eq. (7)). At this stage, oxygen can oxidize Fe^{2+} into Fe^{3+} (Eq. (8)). When the concentration of iron (Fe^{2+} or Fe^{3+}) exceeds the limit of solubility (>10^{-5} M at 5 < pH < 10), iron hydroxides are formed (Eqs. (9) and (10)) thus undergo dehydration (Eqs. (11)–(14)). The oxide scales formed are mostly non-protective layers and responsible of the entrapment of foreign species (including DF) by adsorption (Eq. (15)) and co-precipitation (Eq. (16)) [69] especially under oxic conditions. By increasing the charge transfer between two plated metals, an improvement of iron corrosion occurs followed by MCPs formation. Accordingly, more "free" MCPs products will be available for more DF removal.

$$Fe^0 + H_2O \rightarrow Fe(O)_{ads} + 2H^+ + 2e \quad (2)$$

$$Fe(O)_{ads} + 2H^+ \rightarrow Fe^{2+} + H_2O \quad (3)$$

$$Fe(O)_{ads} + H_2O \rightarrow Fe(OH)_2 \quad (4)$$

$$Fe(O)_{ads} + OH^- \rightarrow HFeO_2^- \quad (5)$$

$$2H^+ + 2e \rightarrow H_2 \quad (6)$$

$$O_2 + 2H_2O + 4e \rightarrow 4OH^- \quad (7)$$

$$Fe^{2+} \rightarrow Fe^{3+} + e \quad (8)$$

$$Fe^{2+} + 2OH^- \rightarrow Fe(OH)_2 \quad (9)$$

$$Fe^{3+} + 3OH^- \rightarrow Fe(OH)_3 \quad (10)$$

$$Fe(OH)_2 \rightarrow FeO + H_2O \quad (11)$$

$$2Fe(OH)_3 \rightarrow Fe_2O_3 + 3H_2O \quad (12)$$

$$4Fe(OH)_3 \rightarrow Fe(OH)_2 + Fe_3O_4 + 5H_2O + (1/2)O_2 \quad (13)$$

$$Fe(OH)_3 \rightarrow FeOOH + H_2O \quad (14)$$

$$FeOOH + DF_{(aq)} \leftrightarrow FeOOH\text{-}(DF) \quad (15)$$

$$DF_{(aq)} + nFe_x(OH)_y^{(3x-y)} \leftrightarrow (DF)[Fe_x(OH)_y^{(3x-y)}]_n \quad (16)$$

In Eqs. (15) and (16), DF = diclofenac and $Fe_x(OH)_y^{(3x-y)}$ = iron hydroxide.

Our results regarding DF removal corroborate with our previous findings on chlorothalonil pesticide that underwent anoxic dechlorination with bimetallics following the decreasing order: PdFe ≫ CuFe > CoFe [53]. Those are also in agreement with Bransfield and co-workers study on the removal of 1,1,1-trichloroethane (1,1,1-TCA) [51]. The reactivity trend noticed was almost similar (PdFe > CuFe) however PdFe is found to be only 2.2 times more reactive than CuFe compared to Fe^0 ([k_{obs} catalyst/k_{obs} Fe] = 3.8 and 8.5) while in the present study, PdFe is proved to be 12.2 times more reactive than CuFe under anoxic conditions ([k_{obs} catalyst/k_{obs} Fe] = 1.9 and 23.2 respectively). In contrast, in the presence of oxygen, the reactivity of PdFe and CuFe was almost similar ([k_{obs} catalyst/k_{obs} Fe] = 3.87 and 4.12 respectively).

3.4. DF reaction products

Table 2 summarizes the chromatographic, UV and MS data of DF and its reaction products identified by HPLC/MS. Fig. 5 shows the MS spectra of all detected DF-related compounds under both (+) and (−) APPI ionization mode. The reaction products can be divided into two categories: (1) Oxidation products for reactions occurring under oxic conditions (DFo: Hydroxylated DF isomers) and (2) reductive products for those occurring under anoxic conditions (DF_1 mono dechlorinated DF; DF_2 fully dechlorinated DF). A deep study of the MS spectra of all reaction products (Fig. 5) was conducted for the identification of all compounds since no authentic standards were available. It has been found that DF (retention time R_t = 8.2 min) presents a molecular ion $[M-H]^-$ at 293.9 m/z with a fragment at 249.9 m/z resulting from a CO_2 neutral loss. DF_1 (R_t = 7.5 min) identified as the mono dechlorinated DF has a molecular ion $[M-H]^-$ at 259.9 m/z and two fragments $[M-CO_2]^-$ and $[M-CO_2-Cl]^-$ at 215.9 and 179.9 m/z respectively. DF_2 (R_t = 5.8 min) shows $[M-H]^-$ at 225.9 m/z and a fragment $[M-HCOO]^-$ at 182.2 m/z confirming the absence of any chlorine atom in its structure in contrast to DF and DF_1 where the isotopic abundance of the chlorine atoms were obvious. DFo (R_t = 4.6 min) shows chlorine isotopic pattern however with a hydroxyl group most probably on the non-chlorinated benzene ring. It shows a molecular ion $[M-H]^-$ at 309.9 m/z and different fragments $[M-H_2O]^-$, $[M-HCOO]^-$ and $[M-HCOO-Cl]^-$ at 293, 266 and 230 m/z respectively. Unfortunately, a last unknown non-chlorinated reaction product DFu (R_t = 10.6 min) presenting a molecular ion $[M-H]^-$ and a corresponding fragment $[M-CO_2]^-$ at 277.0 and 233.0 m/z respectively has not been identified.

As it can be noticed from Table 3, these reaction products were not visible for all bimetallics under both oxic and anoxic conditions which comfort the hypothesis of the adsorption and co-precipitation of DF and its reaction products with the in situ formed MCPs. For example, reaction with Fe did not show any dechlorinated reductive product under anoxic conditions while under oxic conditions, the DFo hydroxylated DF isomers were detected. As for bimetallics, neither CoFe nor SnFe showed reaction products. Also PdFe did not show neither oxidative nor reductive products under oxic conditions while under anoxic conditions DF_1 and DF_2 were clearly discernible. In contrast, NiFe showed the presence of hydroxylated DF (DFo) under oxic conditions while in anoxic solutions none of the reductive products was apparent (DF_1, DF_2). However, CuFe and IrFe were the only two bimetallics showing the presence of DFo reaction products in oxic solutions and the corresponding reductive reaction products (DF_1 and DF_2) under anoxic conditions (Table 3).

3.5. Rationale of the presence and/or the absence of reaction products

It is generally accepted that when MCPs are less abundant, the probability of detecting reaction products in the reactive medium increases [57]. Accordingly, in the absence of oxygen, dehalogenated products appear while in oxidative environment hydroxylated compounds could be detected. Basically, oxidative products should occur at low pH value (<4.5) when microscale iron particles are used [34]. The oxidation reaction is primarily governed by hydroxyl radicals generated via a Fenton's like reaction at the vicinity of in situ formed MCPs. In addition, our results showed that when bimetallics are used instead of Fe^0, hydroxyl radicals could be generated at almost neutral pH as reported above (Section 3.2) and evidenced by the hydroxylated DF reaction products (DFo isomers). The initial pH solution in all experiments were around 7.5–8.5, and dropped by 1.0 to 2.0 units during the first 10 min of reaction, then reached in the range of 6.0–7.5 (Fig. 4). This pH variation is attributed to the fact that reductive dehalogenation by adsorbed hydrogen generates the proton into the solution (Eq. (17)). Once the proton released, it can participate in further reductive reactions such as: formation of (i) H_2 after Fe^0 corrosion (Eq. (18)) or (ii) H_{ads} after reduction on the surface of Me^0 (Eq. (19)). H_{ads} could be released over into the solution as H_2 (Eq. (20)) [70].

$$H_2 + R\text{–}Cl \rightarrow R\text{–}H + H^+ + Cl^- \quad (17)$$

$$Fe^0 + 2H^+ + Fe^{2+} + H_2 \quad (18)$$

$$H^+ + e^- + Me^0 \Leftrightarrow Me^0\text{–}H_{ads} \quad (19)$$

$$Me^0\text{–}H_{ads} + Me^0\text{–}H_{ads} \rightarrow H_2 + 2Me^0 \quad (20)$$

Table 2
UV and MS data of DF and its degradation products in oxic and anoxic solutions observed with Fe^0 and all bimetallic systems used. Transformation products are arranged by decreasing retention time.

Product	R_t (min)[a]	Proposed Structures	Exact Mass g mol^{-1}	UV data (λ_{max}, nm)	Molecular ion and Product ions (relative abundance %) (−) APPI	Molecular ion and Product ions (relative abundance %) (+) APPI	Chemical formula	IUPAC name/(name adopted in the text)
DF_u[c]	10.6	n.d.[b]	278.0	200, 228	$[M-H]^-$ 277.0 (100) $[M-CO_2]^-$ 233.0 (1)	$[M+H]^+$ 279.1 (75.6) n.d.[b] 167.2 (100) n.d.[b] 149.2 (67)	n.d.[b]	n.d.[b]
DF	8.2	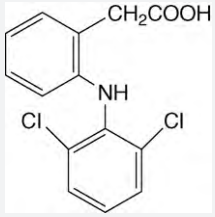	295.0	200, 276	$[M-H]^-$ 293.9 (100) $[M-CO_2]^-$ 249.9 (37)	$[M+H]^+$ 296.0 (100) $[M-H_2O]^+$ 278.1 (13) $[M-H_2O-CO]^+$ 250.1 (11) $[M-H_2O-CO-Cl]^+$ 215.2 (17)	$C_{14}H_{11}Cl_2NO_2$	2-(2-(2,6-dichlorophenylamino)phenyl)acetic acid (DF)
DF_1	7.5	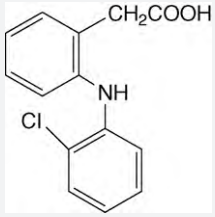	261.0	207, 281	$[M-H]^-$ 259.9 (53) $[M-CO_2]^-$ 215.9 (100) $[M-CO_2-Cl]^-$ 179.9 (3)	$[M+H]^+$ 262.1 (100) $[M-H_2O]^+$ 244.1 (15) $[M-H_2O-CO]^+$ 216.2 (15) $[M-H_2O-CO-Cl]^+$ 181.2 (10)	$C_{14}H_{12}ClNO_2$	2-(2-(2-chlorophenylamino)phenyl)acetic acid (DF_1)
DF_2	5.8	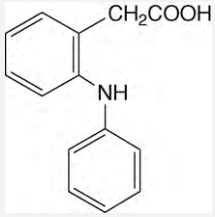	227.0	202, 284	$[M-H]^-$ 225.9 (89) $[M-CO_2-H]^-$ 182.2 (100)	$[M+H]^+$ 228.1 (100) $[M-H_2O]^+$ 210.1 (17) $[M-H_2O-CO]^+$ 182.2 (26)	$C_{14}H_{13}NO_2$	2-(2-(phenylamino)phenyl)acetic acid (DF_2)
DFo	4.6	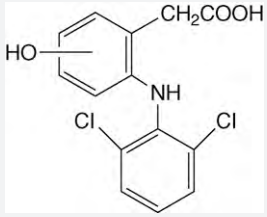	311.0	208, 266	$[M-H]^-$ 309.9 (100) $[M-OH-H]^-$ 293 (5) $[M-CO_2-H]^-$ 266 (70) $[M-CO_2-Cl-H]^-$ 230 (4)	$[M+H]^+$ 312.0 (100) $[M-H_2O]^+$ 294.0 (5) $[M-CO]^+$ 282.0 (21) $[M-CO_2]^+$ 266.0 (11)	$C_{14}H_{11}Cl_2NO_3$	2-(2-(2,6-dichloro-3-hydroxyphenylamino)phenyl)acetic acid (DFo)

Summary of the DF reaction products obtained with Fe^0 and ($Me^0(Fe^0)$) under both oxic and anoxic conditions.

[a] R_t: retention time.

[b] n.d.: not determined.

[c] Unknown.

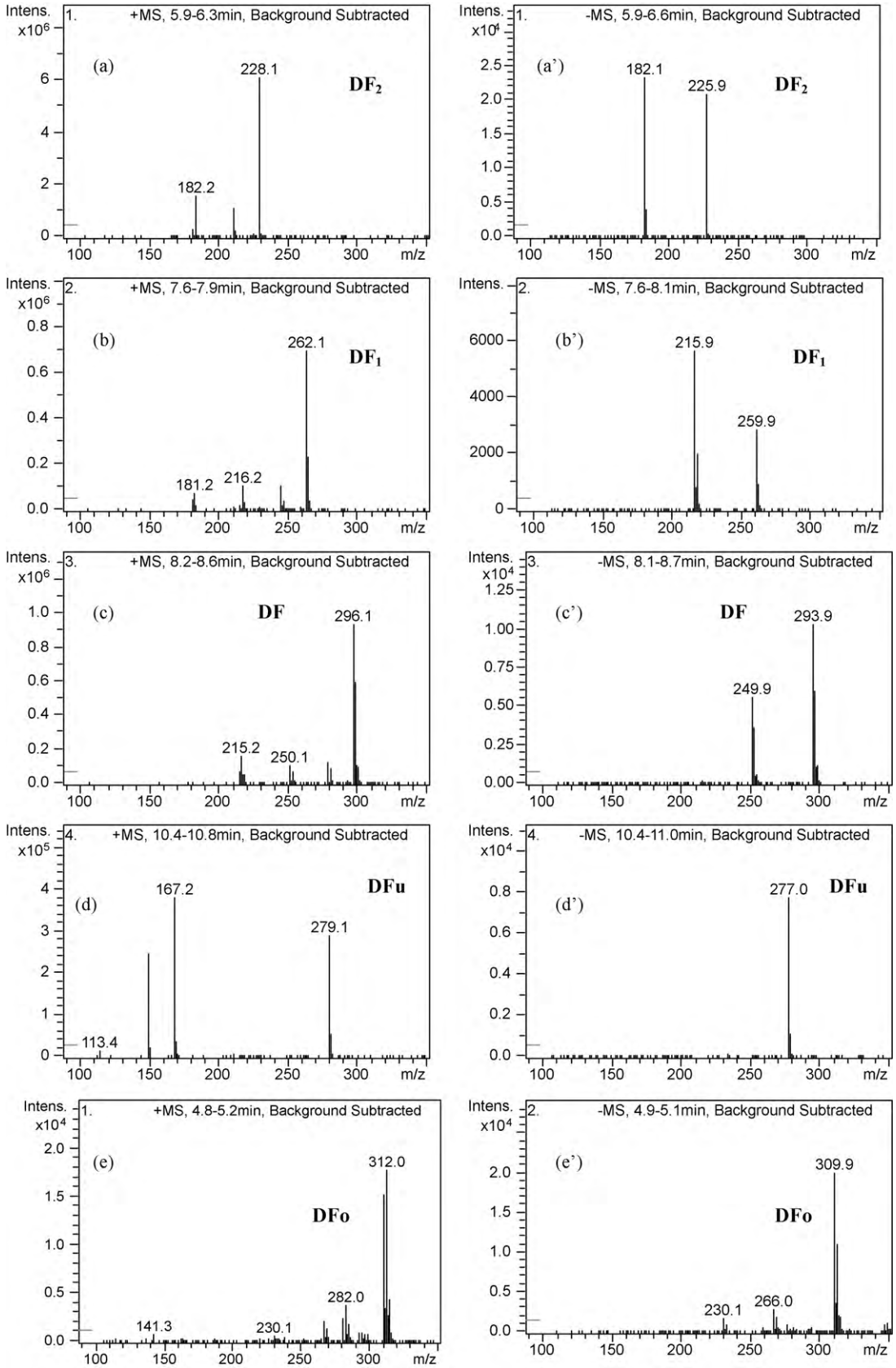

Fig. 5. (a, a′), (b, b′), (c, c′), (d, d′), (e, e′) are the corresponding (+) and (−) APPI/MS spectra of compounds [DF_2], [DF_1], [DF], [DF_u] and [DFo] analyzed in positive and negative ionization modes respectively. All MS characteristic of these compounds are summarized in Table 2.

Table 3
Summary of identified DF reaction products obtained with bimetallic systems under oxic and anoxic conditions.

	By-Products Oxic	Anoxic	Name
Fe	x	–	DFo[b]
Bimetallics			
PdFe	–	x	DF_1[a] DF_2[a]
CuFe	x	x	DF_1[a] DF_2[a] DFo[b]
NiFe	x	–	DFo[b]
CoFe	–	–	–
IrFe	x	x	DF_1[a] DF_2[a] DFo[b]
SnFe	–	–	–

UV and MS data of DF and its degradation products in oxic and anoxic solutions observed with Fe^0 and all bimetallic systems used. Transformation products are arranged by decreasing retention time.
DF_1: monochlorinated DF; DF_2: dechlorinated DF; DFo: Hydroxylated DF
[a] Anoxic
[b] Oxic

Consequently, this might decrease the pH at the interface $Me_1{}^0$(Fe)/solution to less than 4.5 therefore favoring the formation of hydroxyl radicals in the presence of oxygen. Recall that all these observations could not happen without iron corrosion considered the main process responsible of contaminants' removal.

In parallel, when DO is abundant, DF can adsorb onto the surface of iron particles, more particularly on the surface of the in situ formed highly reactive MCPs to form hydrogen peroxide that undergoes Fenton's reaction (Eqs. (21)–(23)), yielding hydroxylated DF isomers. DFo were identified by those slightly different retention times (chromatograms are not shown) and MS spectra showing the same molecular weight with different fragment abundance percentages.

$$(O_2)_{ads} + e \rightarrow O_2^{\bullet -} \quad \text{or} \quad HO_2^{\bullet} \tag{21}$$

$$HO_2^{\bullet} + HO_2^{\bullet} \rightarrow H_2O_2 + O_2 \tag{22}$$

$$Fe^{2+} + H_2O_2 \rightarrow FeOH^{2+} + HO^{\bullet} \tag{23}$$

Finally, the absence of reaction products can be explained by: (i) the formation of MCPs at a case-by-case model of bimetallic systems responsible of the removal of DF reaction products (and even DF itself in oxic solutions) via sequestration/co-precipitation; (ii) the possible adsorption of DF reaction products on MCPs followed by a partial desorption due to a change occurring in the physical properties of the oxide scales under disturbed conditions; (iii) the mineralization of a small part of the original probe after being highly oxidized at the vicinity of MCPs by extremely reactive hydroxyl radicals.

3.6. Characterization of metallic systems (Fe and CuFe)

The formation of iron oxide scales at the surface of metallic iron and bimetallic systems was qualitatively investigated by PIXE and RBS techniques. CuFe was chosen as a representative model of the multiple bimetallic systems tested. PIXE spectra (Fig. 6) showed clearly the presence of Cu at the surface of iron particles just after plating (fresh CuFe) and 2 h after reaction with DF solution under both oxic and anoxic conditions. As it can be noticed, under oxic conditions, the number of X-Rays per μC (relative to Cu) emitted from the used CuFe bimetallics (790 X-rays/μC) is less than the one reported under anoxic conditions (961 X-rays/μC). This difference (171 X-rays/μC) is significant in such analysis knowing that the limit of detection of Cu for PIXE technique is about 8–10 X-rays/μC. As a result, one can conclude that under oxic conditions, an enhanced alteration of the surface of the bimetallic system occurs especially after oxidation in the presence of dissolved molecular oxygen.

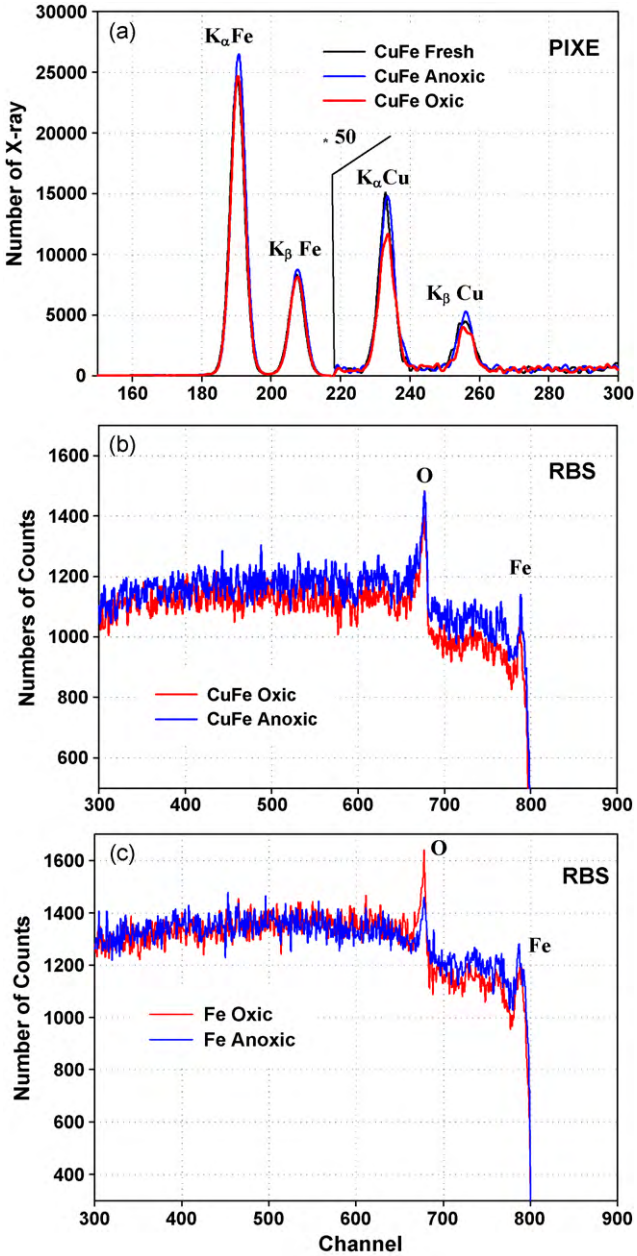

Fig. 6. (a) PIXE and (b) RBS spectra of CuFe bimetallic system (fresh and used in oxic and anoxic solutions). (c) RBS spectra of Fe^0 used (in oxic and anoxic solution). The used metallic particles were collected after 2 h of reaction with DF solution under the same conditions as previously described.

RBS analysis undertaken on the same sample confirmed more oxidation of the CuFe surface by depicting a wider oxygen peak under oxic conditions than in the absence of oxygen (Fig. 6b). Furthermore, RBS spectra showed less iron content for CuFe used in oxic solution than in anoxic medium considered as a reasonable consequence of more iron oxidation. It is also important to notice that even under anoxic conditions, iron corrosion occurs in water however with lesser extent (presence of oxygen peak under

anoxic conditions). This explains the slight DF removal observed in anoxic solutions (20% in anoxic versus 80% in oxic solution, Figs. 1 and 2). The RBS spectra of iron particles showed however improved discrepancy in the oxygen peaks between particles used in oxic and anoxic solutions (Fig. 6c). It corroborates the principle of DF removal enhancement in the presence of oxygen yielding more iron particles corrosion and consequently the formation of a multi particle porous media able to sequestrate and adsorb dissolved contaminants.

4. Conclusions

In this study, it was demonstrated that bimetallic systems successfully remove DF from water and thus could be used for the treatment of DF charged solutions like hospital effluents or hotspots at almost neutral pH values without prior buffering. PdFe was found by far the most powerful system among all bimetallics investigated under anoxic conditions. However, CuFe showed similar high reactivity as PdFe toward DF and can substitute Pd for an effective treatment cost especially under oxic conditions. The latter is proved to be more favorable for the removal of DF via retention and attenuation within the porous scale layer formed during the iron corrosion process. The identification of DF transformation products indicated oxidative reaction products under oxic conditions (DFo) and reductive products under anoxic conditions (DF_1, DF_2 and DF_u). PIXE and RBS surface analyses showed evidence that iron surface oxidation is more improved in oxic solutions. The nature of the metal plated on the surface of iron particles and oxygen abundance into the solution are found to be the key factors determining the reactivity of bimetallics. The elimination mechanism of DF as well as the rate of appearance of reaction products into the solution could be explained by the identity of the plated transition metals and their ability to promote iron corrosion after being oxidized.

Finally plating the same Fe^0 with several more electropositive elements (Co, Cu, Ir, Ni, Pd, Sn) in bimetallic systems is proven a powerful tool to investigate the impact of the kinetics of oxide scale formation and its significance for the Fe^0 reactivity. Results confirmed the prevailing view that the porosity of the oxide scale depends on the relative kinetics of (1) Fe^0 oxidative dissolution, and (2) oxide scale growth. This aspect will be deeply investigated later. Here, Fe^0-based trimetallic systems will be used and the results will be discussed with those presented above.

Acknowledgements

The authors would like to thank the LNCSR and the OGC at AUB for supporting this research under contracts No. 522316 and 888113 respectively. The author is grateful to AUB for the sabbatical leave of absence and to the bureau of cultural affairs and public diplomacy of the American Embassy of Lebanon for awarding 6 months Fulbright scholar at the University of California–Berkeley. The author is also very thankful to Dr. Alice Bejjani from the Lebanese Atomic Energy Commission for her help in analyzing iron particles (PIXE and RBS) and the anonymous reviewers who really helped in improving the quality of this manuscript.

References

[1] A. Kot-Wasik, B. Zukowska, D. Dąbrowska, J. Dębska, J. Pacyna, J. Namieśnik, Physical, chemical, and biological changes in the gulf of gdańsk ecosystem (Southern Baltic sea), Rev. Environ. Contam. Toxicol. 179 (2003) 1–36.
[2] S. Grujić, T. Vasiljević, M. Laušević, Determination of multiple pharmaceutical classes in surface and ground waters by liquid chromatography-ion trap-tandem mass spectrometry, J. Chromatogr. A 1216 (2009) 4989–5000.
[3] J. Radjenović, M. Petrović, F. Ventura, D. Barceló, Rejection of pharmaceuticals in nanofiltration and reverse osmosis membrane drinking water treatment, Water Res. 42 (2008) 3601–3610.
[4] T. Heberer, Tracking persistent pharmaceutical residues from municipal sewage to drinking water, J. Hydrol. 266 (2002) 175–189.
[5] F.F. Sodré, M.A.F. Locatelli, W.F. Jardim, Occurrence of emerging contaminants in Brazilian drinking waters: a sewage-to-tap issue, Water Air Soil Pollut. 206 (2010) 57–67.
[6] T. Okuda, N. Yamashita, H. Tanaka, H. Matsukawa, K. Tanabe, Development of extraction method of pharmaceuticals and their occurrences found in Japanese wastewater treatment plants, Environ. Int. 35 (2008) 815–820.
[7] J.L. Zhou, Z.L. Zhang, E. Banks, D. Grover, J.Q. Jiang, Pharmaceutical residues in wastewater treatment works effluents and their impact on receiving river water, J. Hazard. Mater. 166 (2009) 655–661.
[8] Y. Zhang, S. Geißen, C. Gal, Carbamazepine and diclofenac: removal in wastewater treatment plants and occurrence in water bodies, Chemosphere 73 (2008) 1151–1161.
[9] A.C. Mehinto, E.M. Hill, C.R. Tyler, Uptake and biological effects of environmentally relevant concentrations of the nonsteroidal anti-inflammatory pharmaceutical diclofenac in rainbow trout (*Oncorhynchus mykiss*), Environ. Sci. Technol. 44 (2010) 2176–2182.
[10] S. Suarez, J.M. Lema, F. Omil, Pre-treatment of hospital wastewater by coagulation-flocculation and flotation, Bioresource Technol. 100 (2009) 2138–2146.
[11] L.A. Pérez-Estrada, S. Malato, W. Gernjak, A. Agüera, E.M. Thurman, I. Ferrer, A.R. Fernández-Alba, Photo-fenton degradation of diclofenac: identification of main intermediates and degradation pathway, Environ. Sci. Technol. 39 (2005) 8300–8306.
[12] F.J. Beltrán, J.P. Pocostales, P.M. Alvarez, J. Jaramillo, Mechanism and kinetic considerations of TOC removal from the powdered activated carbon ozonation of diclofenac aqueous solutions, J. Hazard. Mater. 169 (2009) 532–538.
[13] V. Naddeo, V. Belgiorno, D. Ricco, D. Kassinos, Degradation of diclofenac during sonolysis, ozonation and their simultaneous application, Ultrason. Sonochem. 16 (2009) 790–794.
[14] T.L. Johnson, M.M. Scherer, P.G. Tratnyek, Kinetics of halogenated organic compound degradation by iron metal, Environ. Sci. Technol. 30 (1996) 2634–2640.
[15] A. Ghauch, Degradation of benomyl, picloram, and dicamba in a conical apparatus by zero valent iron, Chemosphere 43 (2001) 1109–1117.
[16] A.J. Feitz, S.H. Joo, J. Guan, Q. Sun, D.L. Sedlak, T.D. Waite, Oxidative transformation of contaminants using colloidal zero-valent iron, Colloid Surf. A 265 (2005) 88–94.
[17] C. Noubactep, Characterizing the discoloration of methylene blue in Fe^0/H_2O systems, J. Hazard. Mater. 166 (2009) 79–87.
[18] K.J. Cantrell, D.I. Kaplan, T.W. Wietsma, Zero-valent iron for the in situ remediation of selected metals in groundwater, J. Hazard. Mater. 42 (1995) 201–212.
[19] D.W. Blowes, C.J. Ptacek, S.G. Benner, W.T. Mcrae Che, T.A. Bennett, R.W. Puls, Treatment of inorganic contaminants using permeable reactive barriers, J. Contam. Hydrol. 45 (2000) 123–137.
[20] C. Noubactep, G. Meinrath, P. Dietrich, B. Merkel, Mitigating uranium in ground water: prospects and limitations, Environ. Sci. Technol. 37 (2003) 4304–4308.
[21] J.L. Ginner, P.J.J. Alvarez, S.L. Smith, M.M. Scherer, Nitrate and nitrite reduction by Fe^0: influence of mass transport, temperature, and denitrifying microbes, Environ. Eng. Sci. 21 (2004) 219–229.
[22] H. Sun, L. Wang, R. Zhang, J. Sui, G. Xu, Treatment of groundwater polluted by arsenic compounds by zero valent iron, J. Hazard. Mater. 129 (2006) 297–303.
[23] I.M.C. Lo, C.S.C. Lam, K.C.K. Lai, Hardness and carbonate effects on the reactivity of zero-valent iron for Cr(VI) removal, Water Res. 40 (2006) 595–605.
[24] G.A. Loraine, D.R. Burris, L. Li, J. Schoolfield, Mass transfer effects on kinetics of dibromoethane reduction by zero-valent iron in packed-bed reactors, J. Environ. Eng. 128 (2002) 85–93.
[25] W. Wilopo, K. Sasaki, T. Hirajima, T. Yamanaka, Immobilization of arsenic and manganese in contaminated groundwater by permeable reactive barriers using zero valent iron and sheep manure, Mater. Trans. 49 (2008) 2265–2274.
[26] F.Y. Alshaebi, W.Z.W. Yaacob, A.R. Samsuldin, Sorption on zero-valent iron (ZVI) for arsenic removal, Eur. J. Sci. Res. 33 (2009) 214–219.
[27] P. Rao, P.M.S.H. Mak, T. Liu, K.C.K. Lai, I.M.C. Lo, Effects of humic acid on arsenic(V) removal by zero-valent iron from groundwater with special references to corrosion products analyses, Chemosphere 75 (2009) 156–162.
[28] D.-H. Lim, C.M. Lastoskie, A. Soon, U. Becker, Density functional theory studies of chloroethene adsorption on zerovalent iron, Environ. Sci. Technol. 43 (2009) 1192–1198.
[29] Y.T. He, J.G. Hering, Enhancement of arsenic(III) sequestration by manganese oxides in the presence of iron(II), Water Air Soil Pollut. 203 (2009) 359–368.
[30] J.A. Lackovic, N.P. Nikolaidis, G.M. Dobbs, Inorganic arsenic removal by zero-valent iron, Environ. Eng. Sci. 17 (2000) 29–39.
[31] C. Noubactep, J. Sonnefeld, D. Merten, T. Heinrichs, M. Sauter, Influence of the presence of pyrite and carbonate minerals on the kinetic of the uranium release from a natural rock, J. Radioanal. Nucl. Chem. 270 (2006) 325–333.
[32] C. Noubactep, A. Schöner, G. Meinrath, Mechanism of uranium (VI) fixation by elemental iron, J. Hazard. Mater. 132 (2006) 202–212.
[33] S.H. Joo, A.J. Feitz, T.D. Waite, Oxidative degradation of the carbothioate herbicide, molinate, using nanoscale zero-valent iron, Environ. Sci. Technol. 38 (2004) 2242–2247.

[34] C. Lee, D.L. Sedlak, Enhanced formation of oxidants from bimetallic nickel-iron nanoparticles in the presence of oxygen, Environ. Sci. Technol. 42 (2008) 8528–8533.
[35] H. Song, E.R. Carraway, Catalytic hydrodechlorination of chlorinated ethenes by nanoscale zero-valent iron, Appl. Catal. B: Environ. 78 (2008) 53–60.
[36] Y.H. Tee, L. Bachas, D. Bhattacharyya, Degradation of trichloroethylene and dichlorobiphenyls by iron-based bimetallic nanoparticles, J. Phys. Chem. C 22 (2009) 9454–9464.
[37] Y. Jiao, C. Qiu, L. Huang, K. Wu, H. Ma, S. Chen, L. Ma, L. Wu, Reductive dechlorination of carbon tetrachloride by zero-valent iron and related iron corrosion, Appl. Catal. B: Environ. 91 (2009) 434–440.
[38] L. Xie, C. Shang, Effects of copper and palladium on the reduction of bromate by Fe(0), Chemosphere 64 (2006) 919–930.
[39] C. Noubactep, A. Schöner, P. Woafo, Metallic iron filters for universal access to safe drinking water, Clean—Soil Air Water 37 (2009) 930–937.
[40] C. Noubactep, T. Licha, T.B. Scott, M. Fall, M. Sauter, Exploring the influence of operational parameters on the reactivity of elemental iron materials, J. Hazard. Mater. 172 (2009) 943–951.
[41] C.B. Wang, W.-X. Zhang, Synthesizing nanoscale iron particles for rapid and complete dechlorination of TCE and PCBs, Environ. Sci. Technol. 31 (1997) 2154–2156.
[42] W.X. Zhang, C.B. Wang, H.L. Lien, Treatment of chlorinated organic contaminants with nanoscale bimetallic particles, Catal. Today 40 (1998) 387–395.
[43] W.X. Zhang, Nanoscale iron particles for environmental remediation: an overview, J. Nanopart. Res. 5 (2003) 323–332.
[44] A. Ghauch, H. Abou Assi, A. Tuqan, Investigating the mechanism of clofibric acid removal in Fe^0/H_2O systems, J. Hazard. Mater. 176 (2010) 48–55.
[45] L.J. Matheson, P.G. Tratnyek, Reductive dehalogenation of chlorinated methanes by iron metal, Environ. Sci. Technol. 28 (1994) 2045–2053.
[46] E.J. Weber, Iron-mediated reductive transformations: investigation of reaction mechanism, Environ. Sci. Technol. 30 (1996) 716–719.
[47] S.F. O'Hannesin, R.W. Gillham, Long-term performance of an in situ "Iron Wall" for remediation of VOCs, Ground Water 36 (1998) 164–170.
[48] C. Noubactep, Processes of contaminant removal in Fe0/H2O systems revisited: the importance of co-precipitation, Open Environ. J. 1 (2007) 9–13.
[49] C. Noubactep, A critical review on the process of contaminant removal in Fe^0–H_2O systems, Environ. Technol. 29 (2008) 909–920.
[50] D.C. Harris, Quantitative Chemical Analysis, Freeman and Company, New York, 2007.
[51] D.M. Cwiertny, S.J. Bransfield, K.J.T. Livi, D.H. Fairbrother, A.L. Roberts, Exploring the influence of granular iron additives on 1,1,1-trichloroethane reduction, Environ. Sci. Technol. 40 (2006) 6837–6843.
[52] S.J. Bransfield, D.M. Cwiertny, K. Livi, D.H. Fairbrother, Influence of transition metal additives and temperature on the rate of organohalide reduction by granular iron: implications for reaction mechanisms, Appl. Catal. B: Environ. 76 (2007) 348–356.
[53] A. Ghauch, A. Tuqan, Catalytic degradation of chlorothalonil in water using bimetallic iron-based systems, Chemosphere 73 (2008) 751–759.
[54] A. Ghauch, A. Tuqan, Reductive destruction and decontamination of aqueous solutions of chlorinated antimicrobial agent using bimetallic systems, J. Hazard. Mater. 164 (2009) 665–674.
[55] R.D. Vidic, M.T. Suidan, U.K. Traegner, G.F. Nakhla, Adsorption isotherms: illusive capacity and role of oxygen, Water Res. 24 (1990) 1187–1195.
[56] R.D. Vidic, M.T. Suldan, R.C. Brenner, Oxidative coupling of phenols on activated carbon: impact on adsorption equilibrium, Environ. Sci. Technol. 27 (1993) 2079–2085.
[57] A. Ghauch, A. Tuqan, H. Abou Assi, Antibiotic removal from water: elimination of amoxicillin and ampicillin by microscale and nanoscale iron particles, Environ. Pollut. 157 (2009) 1626–1635.
[58] M. Roumie, B. Nsouli, K. Zahraman, A. Reslan, First accelerator based ion beam analysis facility in Lebanon: development and applications, Nucl. Instrum. Meth. B 219–220 (2004) 389–393.
[59] K.A. Hanold, S.M. Fischer, P.H. Cormia, C.E. Miller, J.A. Syage, Atmospheric pressure photoionization. 1. General properties for LC/MS, Anal. Chem. 76 (2004) 2842–2851.
[60] R. Karuna, A. von Eckardsteina, K. Rentscha, Dopant assisted-atmospheric pressure photoionization (DA-APPI) liquid chromatography-mass spectrometry for the quantification of 27-hydroxycholesterol in plasma, J. Chromatogr. B 877 (2009) 261–268.
[61] C. Noubactep, A.-M.F. Kurth, M. Sauter, Evaluation of the effects of shaking intensity on the process of methylene blue discoloration by metallic iron, J. Hazard. Mater. 169 (2009) 1005–1011.
[62] M. Stratmann, J. Müller, The mechanism of the oxygen reduction on rust-covered metal substrates, Corros. Sci. 36 (1994) 327–359.
[63] C. Noubactep, The suitability of metallic iron for environmental remediation, Environ. Progr. (2010), doi:10.1002/ep.10406.
[64] S. Nesic, Key issues related to modeling of internal corrosion of oil and gas pipelines—a review, Corros. Sci. 49 (2007) 4308–4338.
[65] C. Noubactep, An analysis of the evolution of reactive species in Fe^0/H_2O systems, J. Hazard. Mater. 168 (2009) 1626–1631.
[66] C. Noubactep, On the operating mode of bimetallic systems for environmental remediation, J. Hazard. Mater. 164 (2009) 394–395.
[67] M.S. Odziemkowski, T.T. Schuhmacher, R.W. Gillham, E.J. Reardon, Mechanism of oxide film formation on iron in simulating groundwater solutions: Raman spectroscopic studies, Corros. Sci. 40 (1998) 371–389.
[68] H.A. Moreno-Casillas, D.L. Cocke, J.A.G. Gomes, P. Morkovsky, J.R. Parga, E. Eterson, Electrocoagulation mechanism for COD removal, Sep. Purif. Technol. 56 (2007) 204–211.
[69] C. Noubactep, A. Schöner, Metallic iron for environmental remediation: learning from electrocoagulation, J. Hazard. Mater. 175 (2010) 1075–1080.
[70] J.H. Chang, S.H. Cheng, The remediation performance of a specific electrokinetics integrated with zero-valent metals for perchloroethylene contaminated soils, J. Hazard. Mater. B 131 (2006) 153–162.